European Journal of Pharmaceutics and Biopharmaceutics 158 (2021) 245–253

Contents lists available at ScienceDirect

European Journal of Pharmaceutics and Biopharmaceutics

journal homepage: www.elsevier.com/locate/ejpb

Melt milling as manufacturing method for solid crystalline suspensions

Philip da Igreja [a,b], Annika Erve [b], Markus Thommes [b,*]

[a] INVITE GmbH, Chempark Building W32, 51368 Leverkusen, Germany
[b] Laboratory of Solids Process Engineering, Department of Biochemical and Chemical Engineering, TU Dortmund University, 44227 Dortmund, Germany

ARTICLE INFO

Keywords:
Submicron particles
Annular gap mill
Melt milling
Solid crystalline suspension

ABSTRACT

Production of submicron particles (0.1–1 μm) has been identified by the pharmaceutical industry as a key technology to enhance the bioavailability of poorly water-soluble drugs. However, nanosuspensions derived from commonly applied wet milling suffer from long-term stability issues, making further downstream processing necessary. In previous works, the formulation as a long–term stable solid crystalline suspension (SCS) was introduced, for which the crystalline drug is ground in a (molten) hydrophilic carrier matrix. The model formulation of the antimycotic Griseofulvin and the sugar alcohol Xylitol was reused for comparative purposes. Due to process limitations regarding the degree of comminution, the present work demonstrates the application of fine grinding in the framework of SCS manufacturing. A custom-built mill with annular gap geometry successfully yielded particles in the targeted submicron range. A process optimization study lead to improved energy utilization during grinding, which reduced the necessary grinding time and, thereby, the thermal exposition of the drug. Investigation of solid-state properties of the SCS, via differential scanning calorimetry and x-ray powder diffraction, showed no alteration even for extended grinding times. In dissolution experiments, the melt-milled SCS outperformed its predecessors, although mostly agglomerates were found by SEM imaging in the solidified product. In conclusion, melt milling is a valuable tool to overcome low aqueous solubility.

1. Introduction

Poorly water-soluble active pharmaceutical ingredients (APIs) pose a challenge in the pharmaceutical industry due to their low bioavailability in orally-administered drug products. In order to overcome this limitation, comminution of the drug particles to the submicron region (0.1–1 μm) is a regularly-applied technique [1–6]. Particle size reduction is especially useful for biopharmaceutical classification system (BCS) class II substances, which exhibit high permeability but low solubility. There are multiple factors influencing the desired improvements:

1. The increase of exposed surface area causes higher mass transfers, resulting in a more rapid dissolution as shown by Nernst and Brunner [7,8].
2. Particles below a size of 50 μm are not able to support a large diffusion boundary layer. In this case, the layer thickness is approximately equal to the particle radius or diameter [9]. According to the fundamentals of diffusion established by Fick [10] the dissolution rate is increased with decreasing diffusion layer thickness.
3. As shown by Ostwald [11] and Freundlich [12], the solubility of a drug particle in a liquid is dependent on its curvature. Increasing curvature, i.e. decreasing particle size, leads to an increased dissolution driving force. Multiple calculations have shown that this effect is only significant for particles smaller than 1 μm. [13–15]

Several bottom-up and top-down methods, such as nanoprecipitation [14], spray drying [16], high-pressure homogenization [17], milling [2,3,14,18,19] or a combination of the aforementioned methods [20–24] can be employed. Another promising method is the manufacturing of solid crystalline suspensions (SCS) [25–28] to enhance the bioavailability by embedding a BCS class II drug in a hydrophilic carrier matrix. The latter increases the wettability of the drug [25,29] and usually comes in the form of sugar alcohols, such as Xylitol or Mannitol, while other pharmaceutically acceptable compounds with hydroxy function(s) were also proposed [30]. Additionally, a particle size reduction further amplifies a rapid dissolution. Major advantage over (aqueous) nanosuspensions, where the dispersant needs to be removed by energy intensive processes to retain a usable product, is that drug particles are captured in place after crystallization and cannot

* Corresponding author.
E-mail address: professors.fsv.bci@tu-dortmund.de (M. Thommes).

https://doi.org/10.1016/j.ejpb.2020.11.020
Received 26 May 2020; Received in revised form 16 November 2020; Accepted 24 November 2020
Available online 27 November 2020

undergo further agglomeration. Due to the crystalline state of both components, a SCS is thermodynamically stable, offering a long shelf-life.

In order to achieve a particle size reduction in this work, the drug is ground in a molten sugar alcohol carrier, rather than in water or an organic solvent [31,32]. Consequently, the process described herein, originally introduced by Sleziona [33], shall be called melt milling. Previously, manufacturing of SCS has been carried out by either twin-screw hot-melt extrusion [25,27,30] or air jet co-milling [34]. The former yields dispersed drug particles in a continuous phase of carrier material, the latter, an intimate powder mixture. Disadvantageously, both manufacturing techniques have low grinding capabilities towards the submicron region in common. In the case of SCS containing Griseofulvin, results from these two methods showed 20–30% by volume of the Griseofulvin as being in the submicron region. In twin screw extrusion the extent of dispersive mixing depends, amongst other factors, on the shear rate and melt viscosity [35]. The relatively large gap (screw-screw, screw-barrel), paired with a low melt viscosity (100–200 mPas for pure Xylitol) do not offer sufficient stressing conditions. For conventional air jet co-milling, where only a single substance is processed, agglomeration of the dry drug particle inhibits comminution and often causes a practical grinding limit in the single digit micrometer range with respect to final median particle size. When co-grinding a SCS in particular, additionally carrier is required during the process to reach a high dispersity of both components. This negatively impacts the already low grinding efficiency because selective comminution of the drug is no longer not possible [34].

Although the grinding results are limited, the formulation of Griseofulvin with Mannitol and/or Xylitol as an SCS has shown an effective decrease in dissolution time over the pure component [26,27]. Similarly, SCSs formed by Mannitol or Xylitol containing Efavrienz with a drug load of up to 50 wt% with improved dissolution properties are reported [28]. Apart from Griseofulvin, Reitz [27] also used Itraconazole and Carbamazepin with 25 wt% drug load and a 70:30 Mannitol-Xylitol carrier mixture. This ratio allowed for the generation of coherent extrudates at the die using a process temperature of 100 °C. Supersaturation for over 120 min was only achieved in dissolution experiments with Carbamazepin. An increase in dissolution rate over the pure drug was also reported for both Spironolactone and Phenytoin at 10 wt% drug load by extruding them with Mannitol [25].

The aim of this study is to increase the product performance of SCS containing Griseofulvin and Xylitol by overcoming previous limitations and incorporating an increased fraction of submicron particle using a melt milling process. Therefore, custom equipment, with a focus on the specific process needs, is designed and tested. Using a stress model to optimize the process parameters, the operating point, which offers the best grinding result, is chosen. The obtained product is analyzed regarding its solid-state properties to detect negative side effects of the process. Evaluation of the dissolution performance determines the overall suitability of melt milling.

2. Materials and methods

2.1. Materials

Micronized Griseofulvin (Hawkins, Minneapolis, MN, USA) is classified as a BCS class II substance [36], and therefore represents the target drug class of the process. Its melting point is about 220 °C [37,38]. Xylitol (Xylisorb 300, Roquette, Lestrem, France) was used for the continuous carrier phase and melts at a temperature of about 93–94 °C [39]. Mannitol (Pearlitol 160C, Roquette, Lestrem, France) was employed for the differential scanning calorimetry analysis as an additional sugar alcohol. Spherical zirconium dioxide ($\rho_{GM} = 6000$ kg/m^3) grinding media with diameters of 0.3/0.5/1.0 mm (Zetabeads Plus, Netzsch Vakumix GmbH, Weyhe-Dreye, Germany) were used as received in this study. Sodium dodecyl sulfate (Fluka, Buchs, Switzerland) functioned as a stabilizing agent during particle size measurements.

Table 1
Stress energies of the grinding media (SE_{GM}) used in the optimization study with their corresponding process parameters.

	d_{GM} [mm]			n [1/min]	v_{tip} [m/s]
	0.3	0.5	1.0		
SE_{GM} [10^{-3} Nm]	0.005	–	–	1322 (n_{min})	5.4
	0.023	0.108	0.864	2939	12
	–	0.217	1.734	4163	17
	–	0.397	3.174	5632	23

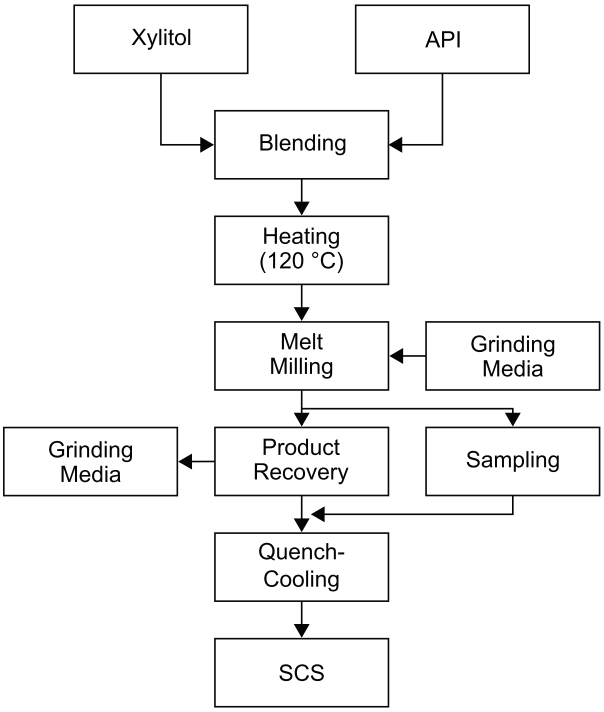

Fig. 1. Process steps for the production of a SCS by melt milling.

2.2. Methods

2.2.1. Manufacturing of SCS

The production of SCS was carried out in a custom-built mill due to the special needs of the process, which cannot necessarily be met with commercially available equipment. Detailed information about the mill can be found in Section 3.1. The micronized drug and the carrier material were blended as a powder in a turbular mixer (TURBULA T 10B, Willy A. Bachofen AG, Muttenz, Switzerland) with 10 wt% drug load. The powder (65 g) was transferred to the milling chamber, heated to 120 °C using the double-jacket and a glycerol-filled thermostat (FP50 HL, Julabo, Seelbach, Germany), so that only Xylitol melted. Afterwards the rotor was inserted and grinding media was added. The filling ratio φ_{GM}, which describes the bulk volume of grinding media in relation to the grinding chamber volume (see Fig. 3) [40], was 80% for all grinding experiments. The motor was then switched on and automatically ramped up in 30 s to the desired speed (see Table 1). Samples were taken at certain specific energy inputs E_m directly from inside the mill without removal of the grinding media. The specific energy is calculated as

$$E_m(t) = \frac{\int_0^{t_{end}} (P(t) - P_0)\, d\tau}{m_{drug}} \quad (1)$$

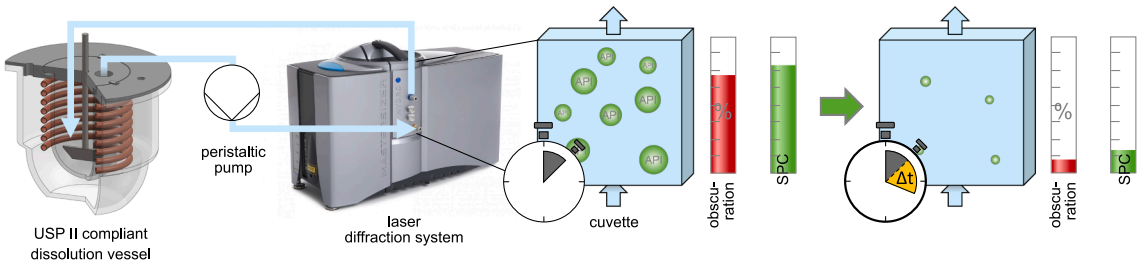

Fig. 2. Schematic of the setup used for measuring the dissolution of crystalline submicron particles based on the change in solid particle concentration (SPC) over time.

The no-load power P_0 was determined prior to each milling experiment after 30–45 min of run time without any filling of the grinding chamber. The power input P(t) during milling was calculated from the shaft torque and speed, which was measured with a torque sensor (4520A10, Kistler, Winterthur, Switzerland). The grinding media inside the end-point sample was removed externally in a custom-built vacuum sieve, rinsed, dried in an oven and reused. Crystallization of all molten samples was realized by quench-cooling at room temperature to create the solidified product. Therefore, about 500 mg of melt was poured on a glass surface and characterized subsequently. A flowchart of the production process can be seen in Fig. 1.

2.2.2. Particle size determination

Particle sizes were measured via laser diffraction (Mastersizer 3000, Malvern Instruments, Malvern, UK) in a wet dispersion unit (Hydro EV). About 60–90 mg of solidified SCS were dispersed in approximately 300 mL of filtered, aqueous, saturated Griseofulvin solution and 3 mL of a 2.5 wt% aqueous SDS solution. This was done in order to strip the Xylitol matrix and release the milled Griseofulvin particles, while the surfactant inhibited agglomeration during the measurement. Alteration of the obtained particle size distribution by SDS was excluded based on preliminary experiments. Sonication and stirring at 2500 1/min were applied during the measurement. All reported particle sizes represent an average of 10 consecutive data points for which a stable particle size distribution (relative standard deviation of $d_{50} \leq 1\%$) was observed. Particle sizes were calculated using Mie-theory, so the complex refractive index of Griseofulvin was set to $1.565 - i\,0.01$ for both light sources (632.8 and 470 nm) accordingly. The real part of the refractive index was determined by the device manufacturer's recommended procedure and is in agreement with the literature [41–43]. The refractive index of the saturated aqueous Griseofulvin solution was determined in an Abbe refractometer (Carl Zeiss, Oberkochen, Germany) at 20 °C to 1.332 and was found to be equal to that of pure water. Small quantities of Xylitol from the sample did not change the refractive index of the dispersant.

2.2.3. Differential Scanning Calorimetry (DSC)

Thermal analysis of 8–10 mg SCS was carried out by differential scanning calorimetry (Q2000, TA Instruments, New Castle, DE, USA) in 40 µL aluminum pans with a heating rate of 10 K/min from 20 to 250 °C, respectively 20–130 °C for pure Xylitol. An identical empty aluminum pan served as a reference. A nitrogen purge flow rate of 50 mL/min was applied. Physical mixtures with 10 wt% drug load were prepared in a batch size of 10 g using a planetary ball mill (Pulverisette 7, Fritsch GmbH, Idar-Oberstein, Germany) with two 20 mm dispersing beads at 400 1/min for 10 min. Premelting of the physical mixture was carried out at 120 °C in an oven (VO29, Memmert GmbH & Co. KG, Schwabach, Germany).

2.2.4. X-Ray Powder Diffraction (XRPD)

The solid-state of the SCS was determined via XRPD (MiniFlex, Rigaku, Tokyo, Japan). Approximately 5 mg samples were placed on a disc of monocrystalline silicon. The acceleration voltage was 40 kV for a 15 mA current. Scanning ranged from $5°/10° \leq 2\theta \leq 30°/50°$ at an increment of 0.02° and a scan speed of 0.125°/s or 0.2°/s. In order to exclude any polymorphs in the SCS, the pure components were also investigated.

2.2.5. Scanning Electron Microscopy (SEM)

The inner microstructure of the SCS was revealed with a scanning electron microscope (H-S4500 FEG, Hitachi High-Technologies Europe, Krefeld, Germany) at 1 kV acceleration voltage using secondary electrons. Therefore, SCS was broken to millimeter sized pieces, which were then fixed to the sample holder with a fracture plane facing upwards to the incident electron beam.

2.2.6. Dissolution kinetics

About 40 mg (sink condition) of sieved SCS (100–200 µm) were dissolved in 900 mL demineralized, degassed water at 37 °C in a USP II apparatus. The solubility c_s of Griseofulvin at 37 °C is 14.67 mg/l [44]. After addition of the sample, the paddle was operated at a speed of 200 1/min for 5 s to quickly produce a uniform dispersion. Afterwards the stirrer speed was reduced to 50 1/min for the duration of the measurement. The mean dissolution time (MDT) was calculated from the dissolution profile $c(t)$ and its maximum value c_{max} by Eq. (2) with the trapezoidal rule.

$$MDT = \frac{\int_0^\infty c_{max} - c(t)dt}{c_{max}} \tag{2}$$

The commonly applied UV/VIS determination of the dissolution profile fails when used with rapidly dissolving nanoparticles, due to residual particles influencing the measurement. Therefore, the dissolved drug fraction was quantified by the change in solid particle concentration (SPC) in a laser diffraction system (Mastersizer 3000, Malvern Instruments, Malvern, UK) (see Fig. 2). This method is based on Anhalt [45], but was adapted for static laser scattering and the standardized dissolution setup according to the pharmacopoeia.

The suspension was pumped at a volume flow rate of 60 mL/min to the cuvette and looped back to the vessel. The laser obscuration, caused by particles absorbing and scattering light, can be related to the SPC in the stream, which was monitored over time (measurement interval ~0.2 Hz). The decrease in SPC between two time points (Δt), called ΔSPC, corresponds to an increase in dissolved drug. Since the dissolved concentration was calculated indirectly from the SPC, only observed changes in SPC can be accounted for. As to not underestimate the dissolved content, due to lag time at the start of the measurement, the final concentration in the dissolution medium was determined by UV/VIS (Jenway 7305, Cole-Parmer, Staffordshire, UK) at 294 nm. The dissolution profile $c(t)$ was then calculated using the obscuration data, the end-point concentration and the method of Anhalt [45].

3. Results

3.1. Mill design

Wet milling at high temperatures (>80 °C) down to the submicron

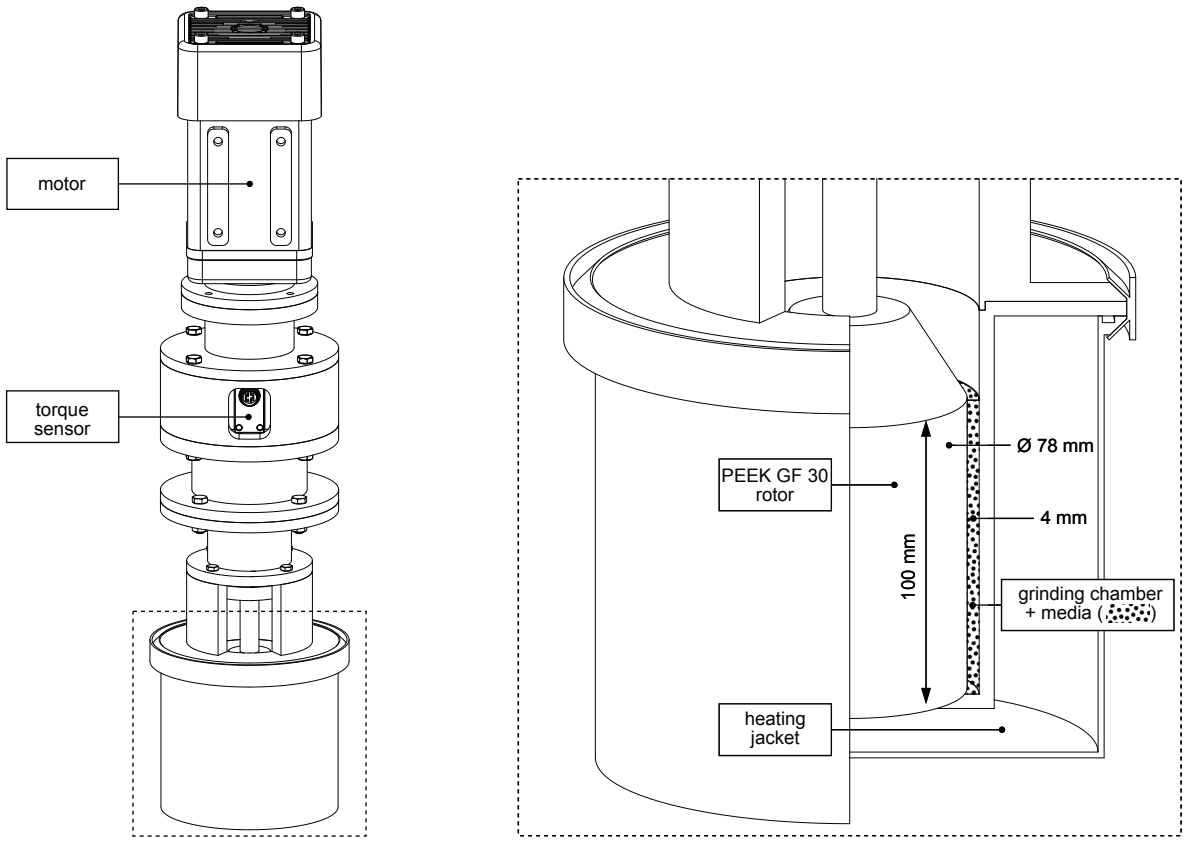

Fig. 3. Drawing of the custom-built annular gap mill used for melt milling of SCS. The grinding chamber volume is highlighted with the grinding media symbolized by black dots.

range is not common, neither in industrial application, nor in research. Hence, there is a lack of literature and suitable equipment meeting pharmaceutical requirements. Therefore, it was necessary to design a custom stirred media mill.

The annular gap geometry offers many advantages for the processing of hot-melts in comparison to discs or pin/counter-pin setups. The main requirement was to minimize the risk of local crystallization on cold spots during grinding, which could otherwise lead to mechanical failure of the equipment. Instead of cooling, which is required in conventional wet milling, constant heating has to be applied. For this, the annular gap type provides a large heating surface to melt volume ratio (here 0.56 mm^2/mm^3 assuming 80% filling ratio), if the gap is small.

Based on the rule-of-thumb that the gap should be approximately 5–20 times the grinding media diameter [40], a gap size of 4 mm was chosen. This spacing is in good agreement with this heuristic for the investigated grinding media diameters.

A rotor diameter of 78 mm gave a desired tip speed of 20 m/s at a reasonable motor frequency (4898 1/min), while maintaining the required 4 mm gap. Such a high tip speed was deemed useful, because potential grinding media dampening, due to an increased melt viscosity, could be counteracted that way. Occurring grinding media dampening would reduce the effective speed of the beads and decrease their available kinetic energy upon collision, limiting the grinding capability of the mill. These insights are also supported by the energy transfer factor, which describes the effectiveness of transferring consumed energy from the mill to the product. Since energy transfer only occurs via adhesion forces in an annular gap mill [46], this parameter corresponds to only 50% of the value for a disc stirrer type mill.

The rotor is made out of polyether ether ketone reinforced with 30% glass-fibre (PEEK GF30, Victrex, Lancashire, UK), to ensure compliance in terms of thermal and mechanical stability. Furthermore, due to its relatively low density, the rotating mass is kept low, and it can be machined conventionally. The stator is made from 1.4571 stainless steel. For commercial application, however, abrasion-resistant ceramics would be a preferred choice.

The length of the rotor is 100 mm giving approximately 100 mL of grinding chamber volume V_{GC}, which is filled with approximately 50 mL of product at a filling ratio of 80% with grinding media. To minimize heat losses, the heating of the double-jacket via a thermostat and a glycerol/water mixture is integrated in the stator. Fig. 3 shows a drawing of the custom-built stirred media.

The critical parts and measures in the final assembly were qualified to be in accordance with the design. Assessment of the annular gap size was carried out with clay at two different heights along the rotor's axis and in four evenly distributed spots for each height. The bottom clearance below the rotor was also verified with clay. The correct operation of the torque sensor was checked by attaching known weights to the outer diameter of the rotor with an inelastic rope and a pulley. The actual motor frequency was measured by a mechanical handheld tachometer (DHZ902, Mayer & Wonisch, Arnsberg, Germany) directly at the motor shaft during operation.

3.2. Process parameter optimization

The grinding efficiency can be strongly impacted by the choice of process parameters. The aim was to find a set of optimal operating conditions with regards to product quality. Here, product quality is described by the particle size distribution, specifically the amount of submicron particles (<1 µm). Consequently, the optimal process parameters yield a high product quality within reasonable grinding times, thus reducing the overall thermal stress on the drug. Simultaneously, contamination with grinding media wear is minimized [47]. For this purpose, the product-related stress model of Kwade was applied [46]. The mean stress energy, which is proportional to the stress energy of the

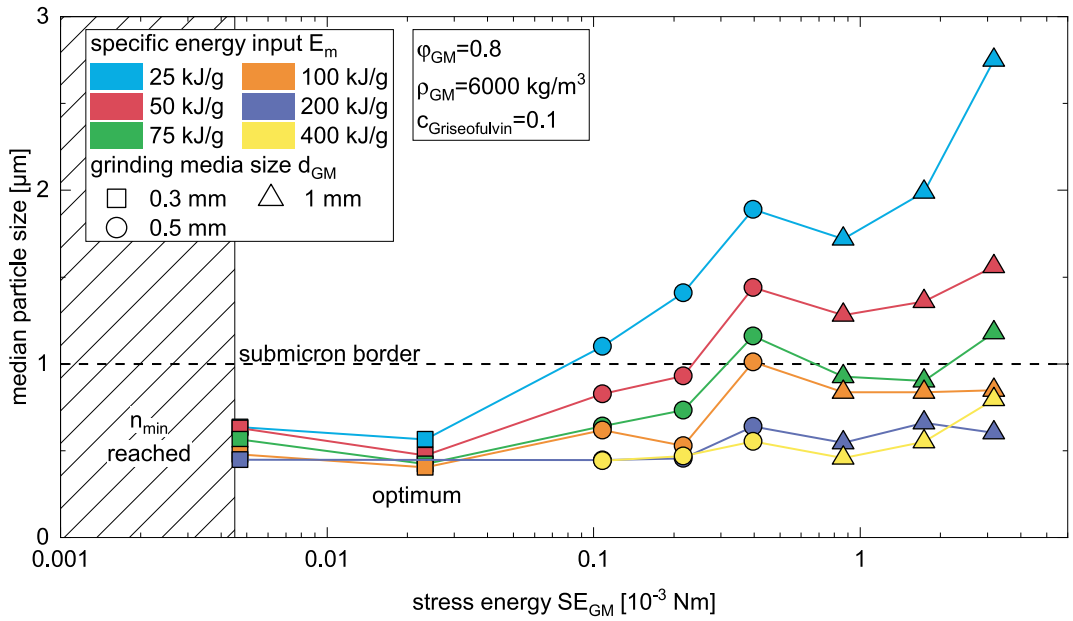

Fig. 4. Median particle size achieved with the custom-built annular gap mill as a function of stress energy of the grinding media. Stress energies in the hatched area could not be realized, due to a minimum motor speed (n_{min}).

grinding media SE_{GM}, was altered by applying different grinding media sizes d_{GM} and tip speeds v_{tip}/motor frequencies n.

$$SE_{GM} = d_{GM}^3 \cdot \rho_{GM} \cdot v_{tip}^2 \quad (3)$$

The influence of the grinding media density ρ_{GM} was not investigated. The theoretical stress energies tested can be found Table 1.

Fig. 4 shows the median particle size of each sample for all conducted grinding experiments over the stress energy for constant specific energy inputs E_m.

It can be seen that for a constant specific energy input after a minimum at $0.023 \cdot 10^{-3}$ Nm the particle size increases with an increase of the stress energy. For high stress energies, the supplied kinetic energy in a breakage event exceeds what is required for a crack to propagate. The surplus is dissipated as heat and in the generation of grinding media wear. Because of the proportionality

$$E_m \propto SN \cdot SE_{GM} \quad (4)$$

an increase in stress energy SE_{GM} leads to a lower number of stress events SN for constant energy input [48], yielding overall larger particles. When decreasing the stress energy below $0.023 \cdot 10^{-3}$ Nm, theoretically a point is reached where not enough energy is supplied for a breakage event to occur, resulting in no comminution at all. However, with the smallest available grinding media and minimum motor frequency, these stress conditions could not be realized (hatched area in Fig. 4). Only a slight increase in median particle size can be observed for $0.005 \cdot 10^{-3}$ Nm. In between those extremes, an optimum can be found, for which just enough kinetic energy is applied. It manifests here as the previously mentioned minimum.

The optimal parameters, found to be a 12 m/s tip speed and 0.3 mm zirconia dioxide grinding media, were used. Under these stress conditions, the initial increase in submicron particles for low specific energy inputs is largest, and the largest amount of submicron particles can be obtained, yielding the highest product quality (see Fig. 6).

Generally, the chosen mill design solves the issue of low submicron particle contents in the manufacturing of SCS, compared with the previously applied manufacturing techniques.

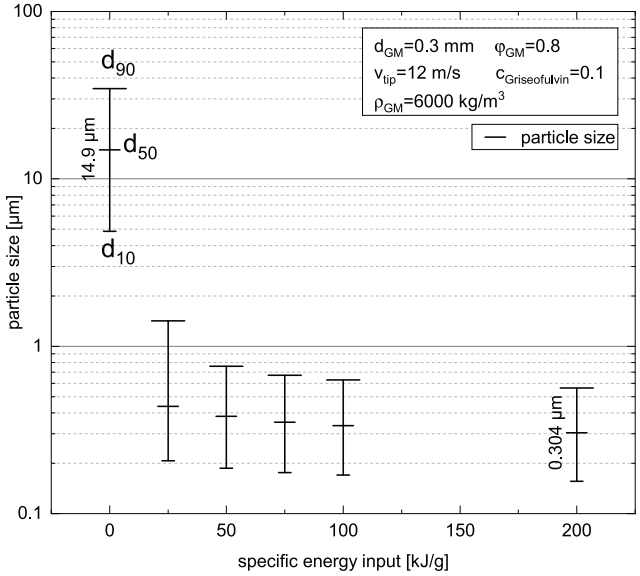

Fig. 5. Evolution of the particle size percentiles (d_{10}, d_{50}, d_{90}) over the specific energy input for grinding with optimal process parameters.

3.3. Grinding results

For the optimal process parameters defined in Section 3.2, a grinding kinetic is presented. Fig. 5 shows a comparison of the most common particle size percentiles of the micronized Griseofulvin starting material and the obtained product for different energy inputs.

The raw material ($d_{50} = 14.9$ µm) has a submicron particle content of 1.3%, which increases to 69.6% at 25 kJ/g ($d_{50} = 0.438$ µm) or about 13 min of grinding (also compare Fig. 6). With further grinding, the overall decrease in particle size is smaller, because the breakage probability for smaller particles is lower [49] and more stress events are necessary. Likewise, the increase in submicron content is slowed down.

Grinding under different stress conditions gave lower initial increases, and longer grinding times were required to accomplish comparable fineness (see Fig. 6). Ultimately, an apparent grinding limit is

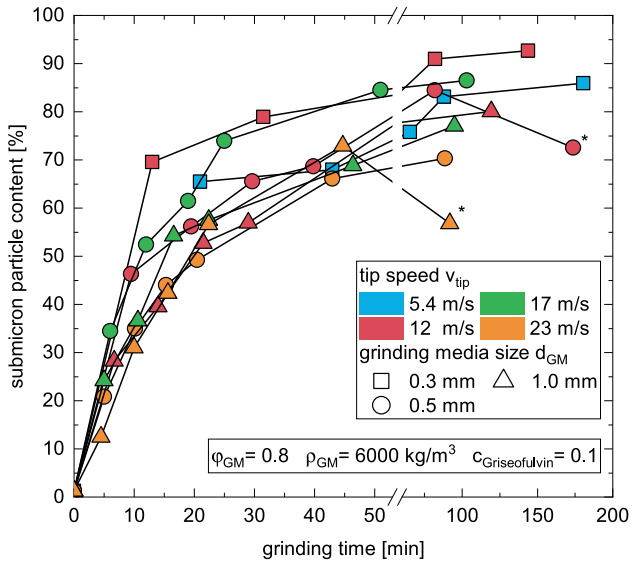

Fig. 6. Achieved submicron particle content over grinding time for different stressing conditions. Marked data points (*) show a decrease in submicron particle content, most likely due to improper sampling.

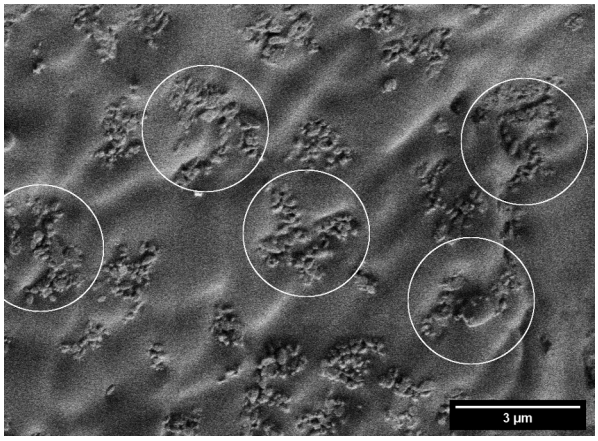

Fig. 7. SEM image of a fracture surface of the solidified SCS. Circles represent a diameter of 3 µm.

reached in Fig. 5, where further energy input does not lead to increased fineness. At that point comminution is negated by agglomeration of drug particles, because on the one hand, the particle-particle interactions increase with decrease in size, and on the other hand, the hydrophobic drug particles are in general not easily wetted by the melt. The grinding kinetics for the optimal process parameters (d_{GM} = 0.3 mm, v_{tip} = 12 m/s) as well as the particle size distribution at 200 kJ/g, are reproducible (d_{50} = 0.298 ± 0.029 µm, n = 3), which is in part due to the narrow stress energy distribution associated with the selected mill type [46], leading to more uniform stress events.

An analysis by scanning electron microscope (SEM) imaging (see Fig. 7) of the solidified SCS revealed the presence of approximately 3 µm agglomerates. Despite the clustering, the primary particles are submicron. The application of stabilizers, such as polymers or surfactants, could lower the grinding limit and reduce agglomeration.

3.4. Solid-state properties of melt milled SCS

In order to evaluate the product performance, the expected increase in dissolution rate should stem from the specific formulation, rather than a change in solid-state properties. Griseofulvin was shown to be susceptible to amorphization during cryogenic milling even for relatively short grinding times [50]. Further, three crystalline polymorphs of Griseofulvin are known [38].

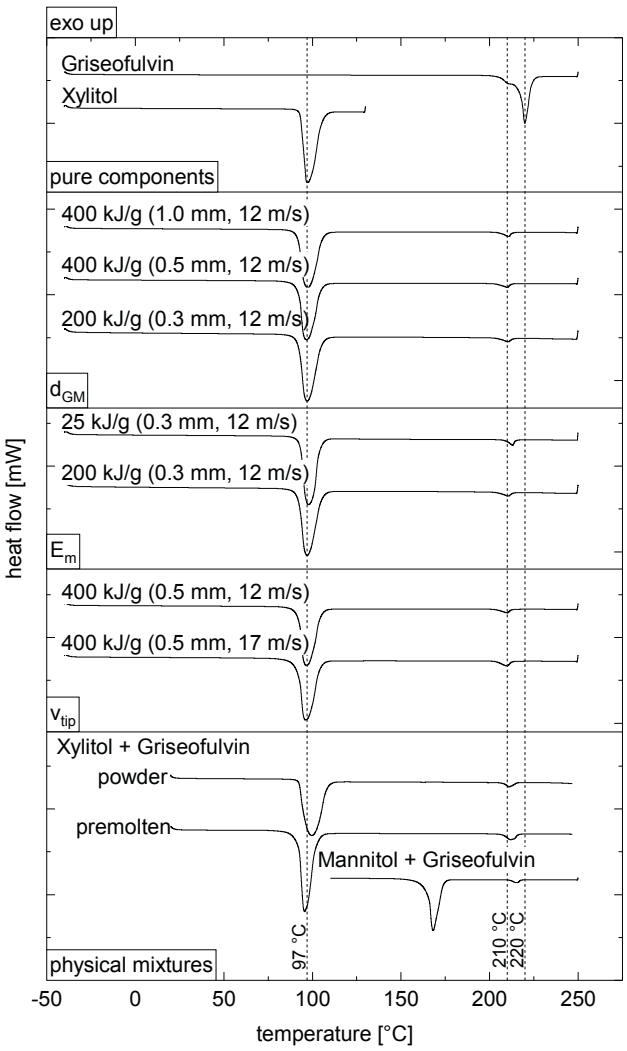

Fig. 8. DSC curves for melt milled SCS under different stress conditions and durations. The pure substances and their respective physical mixtures are shown as well.

Fig. 8 shows the DSC thermogram of SCS samples produces under different stressing conditions, the varied process parameter (d_{GM}, v_{tip} or E_m) is given in the box inside of each segment. Characteristic for a SCS is the presence of discrete melting peaks for the individual substances. Therefore, the pure component peak melting points (Xylitol: 96 °C, Griseofulvin: 220 °C) and a shifted temperature are given as vertical guidelines in Fig. 8 as well. In all tested SCS samples, the individual components (Griseofulvin, Xylitol/Mannitol) can be identified. The second melting peak, belonging to Griseofulvin, is smaller compared to the pure substance, because the drug load is only 10 wt%. The Xylitol exhibits the unchanged melting temperature of the orthorhombic form at 97 °C. Upon visual inspection of the obtained SCS, no yellow/brownish discoloration, caused by caramelization was observed. The underlying oxidation and condensation reactions do not occur at 120 °C [51]. Recrystallization of an amorphous Griseofulvin phase, which occurs between 65 and 123 °C [50], was not observed in the thermograms. This may be due to the process temperature of 120 °C inherently precluding the existence of an amorphous phase during milling.

When comparing the melting peak of Griseofulvin in the SCS with the pure component, a deviation of around 10 °C can be found. Looking at

Table 2
Characteristic properties of Griseofulvin polymorphs. [38]

form	I (stable)	II (metastable)	III (metastable)
characteristic diffraction peak	10.7°	7.2°	7.5°
	21.7°	8.1°	11.5°
melting point	220 °C	214 °C	205 °C

the distinctive properties of the three known Griseofulvin polymorphs (see Table 2), the presence of the metastable forms II and III, which both exhibit a lower melting point than the stable form I, could lead to the observed melting point depression.

XRPD was used to analyze the existence of the metastable forms in the SCS via their characteristic diffraction peaks (see Table 2). With the drug load of 10 wt% only one distinctive peak for form I at 10.7° can be identified from the diffraction patterns given in Fig. 9. The second distinctive Bragg peak at 21.7° is not visible, because the signal intensity is reduced in the SCS. There is no evidence for relevant amounts of form II and III, as the reduction in melting temperature indicates. No amorphous halo is visible for either stress condition, confirming the DSC results of a predominantly crystalline product.

Particle size-dependent melt point depression is known to occur with Griseofulvin nanoparticles and can change the melting point up to 33 K [37]. However, as Fig. 8 (bottom) indicates, the reduction in melting

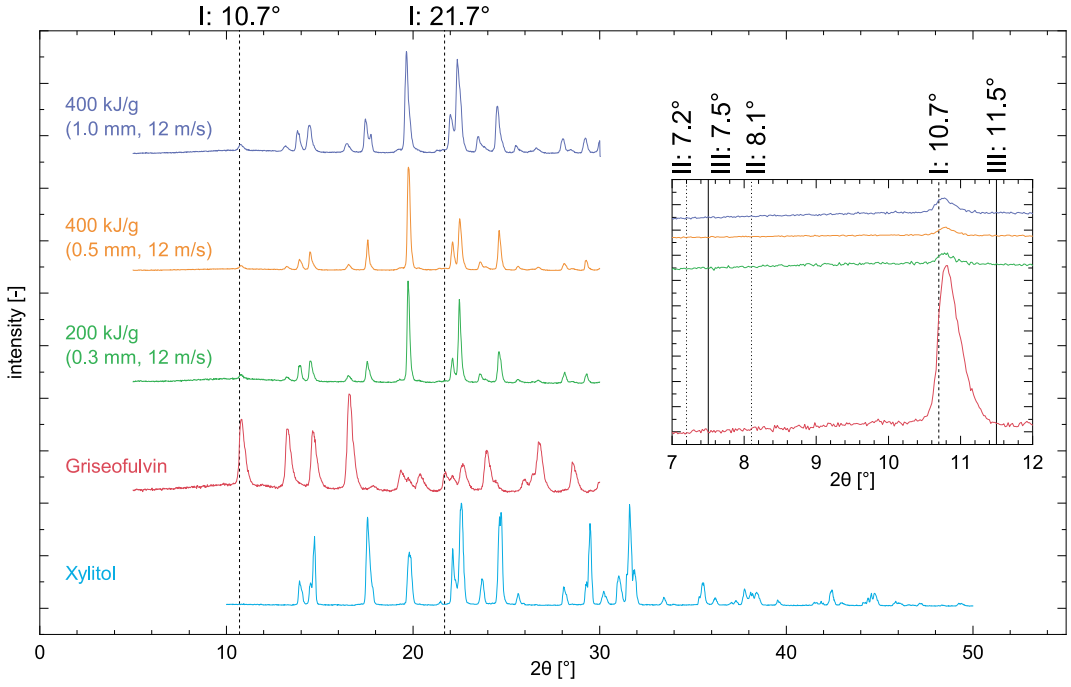

Fig. 9. XRPD diffraction pattern of the pure substances and SCS melt milled with different grinding media sizes and tip speeds. Vertical guidelines refer to the characteristic Bragg peaks of the three known polymorphs (see Table 2).

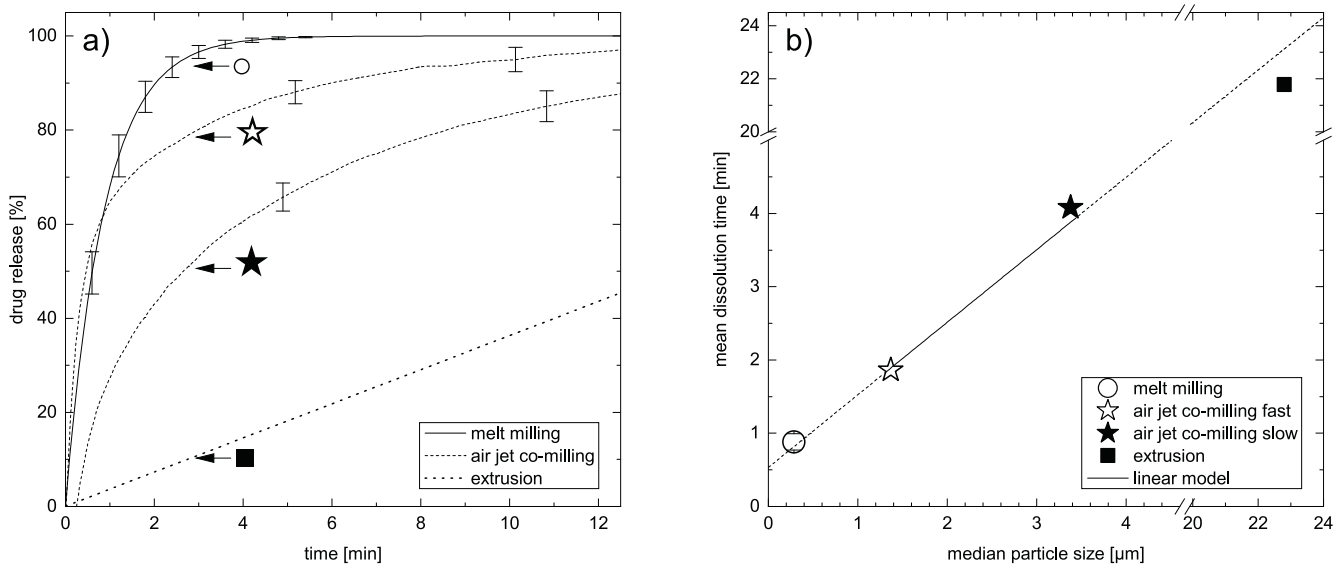

Fig. 10. a) Dissolution kinetics of the melt milled SCS (av ± std, n = 3) compared with SCS from air jet co-milling [34] (av ± std, n = 6) and extrusion [25]. (b) Comparison of mean dissolution times in relation to the achieved median particle size. The dashed line represents an extrapolation of the linear trend, while the symbols correspond to their respective dissolution curves in a).

temperature also occurs in a powderous and a premolten physical mixture of the micronized Griseofulvin and Xylitol (211.00 °C). A physical mixture of Mannitol and Griseofulvin (see Fig. 8 bottom) exhibits lower peak melting-point depression of 215.57 °C, indicating an effect caused by the presence of the carrier material. A solution process of Griseofulvin in the matrix melt, for example, which can be seen as a melting point depression, could be such a phenomenon. A different solubility of Griseofulvin could also explain the varying extend of melting point depression with each sugar alcohol. If the phase diagram rejects a solution process, melting point depression and elevation are also known to occur for particles that are coated or embedded in a matrix [52,53].

In conclusion, there is no evidence for a change of the Griseofulvin solid-state properties related to melt milling. If any dissolution rate enhancements can be achieved in melt milled SCS, it can be purely attributed to the intended effects of the presented process.

3.5. Dissolution kinetics of melt milled SCS

The dissolution kinetics are a formulation's key performance indicator and determine the feasibility of the melt milling process for drugs with low solubility. Therefore, a comparison of the dissolution kinetics for products produced using the different manufacturing technologies of melt milling, air jet co-milling [26] and extrusion [25] was made. It should be noted that the air jet co-milled product used Mannitol instead of Xylitol as a carrier. Since the only effect of the carrier material is to enhance the initial wettability of the hydrophobic drug, it does not impact its further dissolution behavior, because the particle release is effectively instantaneous. This was also shown in a comparison of SCSs from both sugar alcohols with Griseofulvin, where the two release curves were indistinguishable [27].

There are remarkable differences (Fig. 10a) in drug release from SCS at a drug load of 10 wt% when various manufacturing techniques are considered. The slowest release was found for the extruded product, while the fastest was seen for the melt-milled product in this study. Different drug release was observed with the air jet co-milled SCS depending on the operating conditions. The range of drug release is highlighted by two different dissolution curves (air jet co-milling slow, air jet co-milling fast). Mühlenfeld attributed the differences in drug release to differences in drug particles size within the SCS [34]. Therefore, he provided a linear regression model correlating the mean dissolution time (MDT) with the median particle size (based on the volume distribution) from laser diffraction (Fig. 8b). The linear model was extrapolated to larger and smaller particle sizes, and a good agreement for both the melt-milled and the extruded samples was found.

4. Conclusion

The preparation of solid crystalline suspensions containing 90% Xylitol and 10% Griseofulvin in an adapted wet milling process was successfully carried out using a custom-built annular gap mill at 120 °C. Mechanisms known for conventional wet milling apply to melt milling for process optimization. Such optimization leads to short grinding times with improved product quality. The solid-state properties of Griseofulvin were not altered by melt milling even for prolonged grinding times. A submicron particle content of 90% can be achieved in the grinding limit, resulting in an increased dissolution rate, and thereby outperforming the previously applied manufacturing techniques of extrusion and air jet co-milling. Although the primary particles are submicron, agglomerates are present both in the matrix and also upon release in water, which poses a potential limit to the binary formulation. Despite this limitation, the manufacturing of SCS via melt milling offers a new pathway for enhancing the bioavailability of BCS II drugs in a stable, one-step process.

Declaration of Competing Interest

The authors declare that they have no known competing financial interests or personal relationships that could have appeared to influence the work reported in this paper.

Acknowledgments

The authors would like to thank INVITE GmbH for financial support, Sara Jacob for working on the dissolution and Volker Brandt (Biomaterial and Polymer Science, TU Dortmund) for capturing SEM images.

References

[1] A. Afolabi, O. Akinlabi, E. Bilgili, Impact of process parameters on the breakage kinetics of poorly water-soluble drugs during wet stirred media milling: a microhydrodynamic view, Eur. J. Pharm. Sci.: Off. J. Eur. Fed. Pharm. Sci. 51 (2014) 75–86, https://doi.org/10.1016/j.ejps.2013.09.002.
[2] A. Bitterlich, et al., Challenges in nanogrinding of active pharmaceutical ingredients, Chem. Eng. Technol. 37 (5) (2014) 840–846, https://doi.org/10.1002/ceat.201300697.
[3] A. Bitterlich, et al., Process parameter dependent growth phenomena of naproxen nanosuspension manufactured by wet media milling, Eur. J. Pharm. Biopharm.: Off. J. Arbeitsgemeinschaft fur Pharmazeutische Verfahrenstechnik e.V 92 (2015) 171–179, https://doi.org/10.1016/j.ejpb.2015.02.031.
[4] M. Juhnke, J. Berghausen, C. Timpe, Accelerated formulation development for nanomilled active pharmaceutical ingredients using a screening approach, Chem. Eng. Technol. 33 (9) (2010) 1412–1418, https://doi.org/10.1002/ceat.201000062.
[5] J.P. Möschwitzer, Drug nanocrystals in the commercial pharmaceutical development process, Int. J. Pharm. 453 (1) (2013) 142–156, https://doi.org/10.1016/j.ijpharm.2012.09.034.
[6] B. van Eerdenbrugh, G. van den Mooter, P. Augustijns, Top-down production of drug nanocrystals: nanosuspension stabilization, miniaturization and transformation into solid products, Int. J. Pharm. 364 (1) (2008) 64–75, https://doi.org/10.1016/j.ijpharm.2008.07.023.
[7] E. Brunner, Reaktionsgeschwindigkeit in heterogenen Systemen, Zeitschrift für Physikalische Chemie 47U (1) (1904), https://doi.org/10.1515/zpch-1904-4705.
[8] W. Nernst, Theorie der Reaktionsgeschwindigkeit in heterogenen Systemen, Zeitschrift für Physikalische Chemie 47U (1) (1904), https://doi.org/10.1515/zpch-1904-4704.
[9] C. Galli, Experimental determination of the diffusion boundary layer width of micron and submicron particles, Int. J. Pharm. 313 (1–2) (2006) 114–122, https://doi.org/10.1016/j.ijpharm.2006.01.030.
[10] A. Fick, Ueber diffusion, Ann. Phys. Chem. 170 (1) (1855) 59–86, https://doi.org/10.1002/andp.18551700105.
[11] W. Ostwald, Über die vermeintliche Isomerie des roten und gelben Quecksilberoxyds und die Oberflächenspannung fester Körper, Zeitschrift für Physikalische Chemie 34U (1) (1900), https://doi.org/10.1515/zpch-1900-3431.
[12] H. Freundlich, Kapillarchemie, eine Darstellung der Chemie der Kolloide und verwandter Gebiete, Akademische Verlagsgesellschaft, 1922.
[13] D.R. Ely, R. Edwin García, M. Thommes, Ostwald–Freundlich diffusion-limited dissolution kinetics of nanoparticles, Powder Technol. 257 (2014) 120–123, https://doi.org/10.1016/j.powtec.2014.01.095.
[14] R. Shegokar, R.H. Müller, Nanocrystals: industrially feasible multifunctional formulation technology for poorly soluble actives, Int. J. Pharm. 399 (1–2) (2010) 129–139, https://doi.org/10.1016/j.ijpharm.2010.07.044.
[15] C. Brough, R.O. Williams, Amorphous solid dispersions and nano-crystal technologies for poorly water-soluble drug delivery, Int. J. Pharm. 453 (1) (2013) 157–166, https://doi.org/10.1016/j.ijpharm.2013.05.061.
[16] A. Dobrowolski, et al., Preparation of submicron drug particles via spray drying from organic solvents, Int. J. Pharm. 567 (2019) 118501, https://doi.org/10.1016/j.ijpharm.2019.118501.
[17] R.H. Müller, R. Becker, B. Kruss, K. Peters, Pharmaceutical nanosuspensions for medicament administration as system with increased saturation solubility and rate of solution, WO 96/14830, May 23, 1996.
[18] G.B. Romero, C.M. Keck, R.H. Müller, Simple low-cost miniaturization approach for pharmaceutical nanocrystals production, Int. J. Pharm. 501 (1–2) (2016) 236–244, https://doi.org/10.1016/j.ijpharm.2015.11.047.
[19] F. Stenger, S. Mende, J. Schwedes, W. Peukert, Nanomilling in stirred media mills, Chem. Eng. Sci. 60 (16) (2005) 4557–4565, https://doi.org/10.1016/j.ces.2005.02.057.
[20] J. Salazar, R.H. Müller, J.P. Möschwitzer, Combinative particle size reduction technologies for the production of drug nanocrystals, J. Pharm. 2014 (2014) 265754, https://doi.org/10.1155/2014/265754.
[21] K. Šimková, B. Joost, G. Imanidis, Production of fast-dissolving low-density powders for improved lung deposition by spray drying of a nanosuspension, Eur. J. Pharm. Biopharm.: Off. J. Arbeitsgemeinschaft fur Pharmazeutische Verfahrenstechnik e.V 146 (2020) 19–31, https://doi.org/10.1016/j.ejpb.2019.11.003.
[22] R.H. Müller, J.P. Möschwitzer, Method and device for producing very fine particles and coating such particles, US2009/0297565 A1, Dec 3, 2009.

[23] J.P. Möschwitzer, Method for producing ultrafine submicronic suspensions, WO2006/094808 A3, Sep 14, 2006.
[24] J.P. Möschwitzer, Method for carefully producing ultrafine particle suspensions and ultrafine particles and use therof, WO 2006/108637 A2, Oct 19, 2006.
[25] M. Thommes, D.R. Ely, M.T. Carvajal, R. Pinal, Improvement of the dissolution rate of poorly soluble drugs by solid crystal suspensions, Mol. Pharm. 8 (3) (2011) 727–735, https://doi.org/10.1021/mp1003493.
[26] C. Muehlenfeld, B. Kann, M. Windbergs, M. Thommes, Solid dispersion prepared by continuous cogrinding in an air jet mill, J. Pharm. Sci. 102 (11) (2013) 4132–4139, https://doi.org/10.1002/jps.23731.
[27] E. Reitz, Extrudierte feste Dispersionen zur Verbesserung, Heinrich-Heine-Universität Düsseldorf, 2014.
[28] J.N. Pawar, R.A. Fule, M. Maniruzzaman, P.D. Amin, Solid crystal suspension of Efavirenz using hot melt extrusion: Exploring the role of crystalline polyols in improving solubility and dissolution rate, Mater. Sci. Eng. C, Mater. Biol. Appl. 78 (2017) 1023–1034, https://doi.org/10.1016/j.msec.2017.04.055.
[29] T. van Duong, G. van den Mooter, The role of the carrier in the formulation of pharmaceutical solid dispersions. Part I: crystalline and semi-crystalline carriers, Expert Opinion Drug Delivery 13 (11) (2016) 1583–1594, https://doi.org/10.1080/17425247.2016.1198768.
[30] M. Thommes, R. Pinal, M.T. Carvajal, Solid formulations of crystalline compounds, CA 02702935.
[31] C. Knieke, C. Steinborn, S. Romeis, W. Peukert, S. Breitung-Faes, A. Kwade, Nanoparticle production with stirred-media mills: opportunities and limits, Chem. Eng. Technol. 33 (9) (2010) 1401–1411, https://doi.org/10.1002/ceat.201000105.
[32] M. Nöske, S. Breitung-Faes, A. Kwade, Electrostatic stabilization and characterization of fine ground silicon particles in ethanol, Silicon 11 (6) (2019) 3001–3010, https://doi.org/10.1007/s12633-019-0089-0.
[33] D. Sleziona, T. Gottschalk, Schmelzmahlung als Methode zur Erhöhung der Löslichkeit schwer löslicher Arzneistoffe, ProcessNet Neuss (2018).
[34] C. Mühlenfeld, Herstellung fester Dispersionen durch Covermahlung in einer Luftstrahlmühle, Heinrich-Heine-Universität Düsseldorf, 2013.
[35] K. Kohlgrüber (Ed.), Co-Rotating Twin-Screw Extruders: Fundamentals, Carl Hanser Verlag GmbH & Co. KG, München, 2019.
[36] World Health Organization, WHO Technical Report Series.
[37] P. Bergese, I. Colombo, D. Gervasoni, L.E. Depero, Melting of nanostructured drugs embedded into a polymeric matrix, J. Phys. Chem. B 108 (40) (2004) 15488–15493, https://doi.org/10.1021/jp048762u.
[38] A. Mahieu, et al., On the polymorphism of griseofulvin: identification of two additional polymorphs, J. Pharm. Sci. 102 (2) (2013) 462–468, https://doi.org/10.1002/jps.23349.
[39] A. Raemy, T.F. Schweizer, Thermal behaviour of carbohydrates studied by heat flow calorimetry, J. Therm. Anal. 28 (1983) 95–108.
[40] A. Kwade, J. Schwedes, Wet Comminution in Stirred Media Mills, KONA 15 (1997) 91–102, https://doi.org/10.14356/kona.1997013.
[41] H.-J.R. Martin, Charakterisierung von schwerlöslichen Arnzeistoff-Nanopartikeln.
[42] A. Watanabe, Y. Yamaoka, E. Akaho, K. Kuroda, T. Yokoyama, T. Umeda, Study of crystalline drugs by means of a polarizing microscope. VI. Polarizing microscopy of drugs acting on the nervous system and on individual organs listed in the Japanese Pharmacopoeia X, Chem. Pharm. Bull. 33 (4) (1985) 1599–1608, https://doi.org/10.1248/cpb.33.1599.
[43] X. Cao, B.C. Hancock, N. Leyva, J. Becker, W. Yu, V.M. Masterson, Estimating the refractive index of pharmaceutical solids using predictive methods, Int. J. Pharm. 368 (1–2) (2009) 16–23, https://doi.org/10.1016/j.ijpharm.2008.09.044.
[44] R. Paus, Y. Ji, L. Vahle, G. Sadowski, Predicting the solubility advantage of amorphous pharmaceuticals: A novel thermodynamic approach, Mol. Pharm. 12 (8) (2015) 2823–2833, https://doi.org/10.1021/mp500824d.
[45] K. Anhalt, S. Geissler, M. Harms, M. Weigandt, G. Fricker, Development of a new method to assess nanocrystal dissolution based on light scattering, Pharm. Res. 29 (10) (2012) 2887–2901, https://doi.org/10.1007/s11095-012-0795-4.
[46] A. Kwade, A stressing model for the description and optimization of grinding processes, Chem. Eng. Technol. 26 (2) (2003) 199–205, https://doi.org/10.1002/ceat.200390029.
[47] M. Juhnke, D. Märtin, E. John, Generation of wear during the production of drug nanosuspensions by wet media milling, Eur. J. Pharm. Biopharm.: Off. J. Arbeitsgemeinschaft fur Pharmazeutische Verfahrenstechnik e.V 81 (1) (2012) 214–222, https://doi.org/10.1016/j.ejpb.2012.01.005.
[48] A. Kwade, J. Schwedes, Chapter 6 wet grinding in stirred media mills, in: Handbook of Powder Technology, Elsevier, Particle Breakage, 2007, pp. 251–382.
[49] S.L.A. Hennart, P. van Hee, V. Drouet, M.C. Domingues, W.J. Wildeboer, G.M. H. Meesters, Characterization and modeling of a sub-micron milling process limited by agglomeration phenomena, Chem. Eng. Sci. 71 (2012) 484–495, https://doi.org/10.1016/j.ces.2011.11.010.
[50] N.S. Trasi, S.R. Byrn, Mechanically induced amorphization of drugs: a study of the thermal behavior of cryomilled compounds, AAPS PharmSciTech 13 (3) (2012) 772–784, https://doi.org/10.1208/s12249-012-9801-8.
[51] K.K. Mäkinen, Biochemical Principles of the Use of Xylitol in Medicine and Nutrition with Special Consideration of Dental Aspects, Birkhäuser Basel, Basel, 1978.
[52] N.X. Sun, H. Lu, Y.C. Zhou, Explanation of the melting behaviour of embedded particles; equilibrium melting point elevation and superheating, Philos. Mag. Lett. 76 (2) (1997) 105–110, https://doi.org/10.1080/095008397179282.
[53] J. Zhong, Superheating of Ag nanoparticles embedded in Ni matrix, Acta Mater. 49 (15) (2001) 2897–2904, https://doi.org/10.1016/S1359-6454(01)00212-9.